FAULT LOCATION ALGORITHM FOR PRIMARY DISTRIBUTION FEEDERS BASED ON VOLTAGE SAGS

Rodrigo A. F. Pereira[1], Mladen Kezunovic[2] and José R. S. Mantovani[1]
[1]Universidade Estadual Paulista – FEIS/UNESP
Ilha Solteira, São Paulo, Brazil
[2]Texas A&M University
College Station, Texas, USA
ddigo@yahoo.com, kezunov@ece.tamu.edu, mant@dee.feis.unesp.br

Abstract –Aiming at reaching the best quality in terms of supplying and services, some utilities are using more and more automation and instrumentation devices in its networks. Thus, in a new scenario, voltage sags are available from some additional measurements along the feeder by means of power quality or voltage measurement devices. In this work, a fault location algorithm, which uses voltage sag measurements, for primary distribution feeders is proposed. Preliminary tests performed on large-scale practical feeders using a generic load modeling show that the proposed algorithm is robust and suitable for carrying out fault location with improved accuracy.

Keywords: Fault location, distribution feeders, voltage sag

1 INTRODUCTION

The competitiveness in the electric power market and the increasing exigency for the electric utilities keep the supply and the power quality indices within the required standards have gotten the attention for the development of techniques as well as control and measurement devices in order to enhance the reliability indices of the distribution power systems. In this context, the fast and efficient fault location on distribution feeders is one way for improving such indices. Thus, the fault location issue is widely investigated at several research center and different fault location techniques have been proposed presenting results that show the necessity of new investments and new studies related to this issue.

Among the main difficulties, which degrade the accuracy and the quality of practical results, presented for the majority of proposed techniques for fault location in overhead distribution feeders could be cited: the feeder topology and the impedance variations due to network reconfigurations; the loading levels, which directly affect the pre-fault voltages and currents; line sections presenting different conductor sizes; and the exactly knowledge of the source impedance.

Several methodologies and techniques for fault location on distribution feeders have been proposed [2], [5] – [8], [10], and [12] – [13]. These proposals for fault location are basically different due to the employed methodology or technique, number of variables, and instrumentation required for the fault location process. Bigger the amount of information related to the network, and pre- and during-fault conditions, more accurate the fault location results and consequently bigger the complexity of the technique or methodology for fault location.

The adoption of a fault location technique or methodology to be implemented in an electric utility is related to the availability of measurement and control devices installed on the feeder as well as the utility planning for purchasing the required devices and software. Thus, among other factors, in the making-decision process a suitable cost-benefit relationship should considerer the financial resources to be invested and the benefits achieved for both utilities and customers. The benefits for the utilities are the reduction of costs for fault location and network repairs, and the benefits for the customers are maintenance of the supply quality and reduction of the outage duration.

The fault location algorithm herein proposed is based on [1], [10] – [12] that are efficient solutions when voltage and current measurements are available. In this technique the employed quantities are the pre- and during-fault voltage and current phasors of fundamental frequency measured at the feeder root node, as well as the voltage sag magnitudes measured at some feeder nodes.

In order to assess the efficiency of the proposed fault location technique, simulation and results are presented for an overhead, 13.8 kV, 238-node practical feeder.

Following, the fault location algorithm is presented in section 2. The simulation results and discussions are presented in section 3. Finally, conclusions are presented in section 4.

2 FAULT LOCATION ALGORITHM

Most of overhead distribution networks present radial topology, several line sections, three-, two- and single-phase laterals, different load types and low *X/R* ratio. Different of transmission lines, distribution networks are non-transposed and unbalanced. Thus, a fault location algorithm should be able to deal with these characteristics employing suitable techniques for analyzing these networks. The proposed algorithm is based on these premises and on the backward/forward load flow algorithm presented in [3] that is suitable and efficient to analyze distribution networks.

The proposed algorithm is based on the different magnitude of voltage sag for each feeder node during a fault. Thus, the usage of sparse voltage measurements along the feeder allows the algorithm to reach the suit-

able accuracy for indicating the area or even the fault location. Figure 1 illustrates the block diagram of the fault location algorithm.

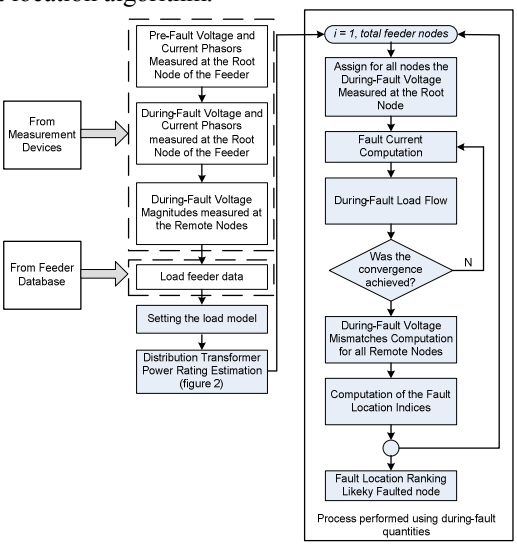

Figure 1: Block diagram of the algorithm.

The algorithm requires information stored in database and pre- and during-fault quantities recorded in order to carry out the fault location. Following, the main points of the proposed algorithm are detailed.

2.1 Electric quantities

Pre- and during-fault phasors of voltages and currents as well as magnitudes of voltage sags during the fault recorded at some nodes are required by the algorithm to carry out fault location.

2.1.1 Pre-fault phasors of voltage and current

Fundamental frequency pre-fault phasors of voltage and current should be recorded at the root node of the faulted feeder. These phasors are used in the calculation of the total pre-fault complex power. This power is used for estimating the loading of each feeder transformer, as will be presented in subsection 2.4.

2.1.2 During-fault phasors of voltage and current

Fundamental frequency during-fault phasors of voltage and current are also recorded at the root node of the faulted feeder. These phasors are used for the algorithm in order to carry out fault location, as will be seen in subsections 2.5 to 2.8.

2.1.3 During-fault voltage sag magnitudes

In addition to the pre- and during-fault phasors, the fault location algorithm uses the voltage sag magnitudes sparsely measured at some feeder nodes. As described in subsection 2.7 later, these quantities are the main information for the algorithm to determine the likely area or location of the fault.

2.2 Feeder database

Feeder database is composed by topological information such as line section length, transformer and protective device locations as well as electric information such as line section impedances and nominal power of transformers.

2.3 Load modeling

The loads of a distribution system are generally specified by its demand power. In this work, a generic static load model presented in [9], given by (1), is used in the fault location algorithm.

$$\mathbf{S} = P_n \cdot \left(\frac{V}{V_n}\right)^{np} + jQ_n \cdot \left(\frac{V}{V_n}\right)^{nq} \quad (1)$$

where:

P_n: Nominal active power;

Q_n: Nominal reactive power;

V: Nodal voltage magnitude;

V_n: Nominal voltage of the load;

np: Active power exponent;

nq: Reactive power exponent.

Constant power loads are represented using $np = nq = 0$. Constant current loads are represented using $np = nq = 1$. Constant impedance loads are represented using $np = nq = 2$.

For composite system loads, the exponent np usually ranges between 0.5 and 1.8; the exponent nq usually ranges between 1.5 and 6. In the absence of specific information, the most commonly accepted values for np is 1.0 (constant current power) and for nq is 2.0 (constant impedance power) [9].

2.4 Transformer power rating estimation

The calculation of the exact loading of transformers is not a straightforward accomplishment. Thus, for fault location purposes, the errors introduced in the results by approximated loading of transformers are generally smaller than the errors introduced by the divergence between the used load model and the actual load model. Then, in order to calculate the transformer power rating an iterative approach is proposed. Thus, for the *n-th* iteration, the transformer power rating ($\mathbf{S}_i^n$) is computed as follows:

$$\mathbf{S}_i^n = \left(\lambda_i S_i^{nom} \frac{S_{calc}}{\sum_{k=1}^{nt} \lambda_k S_k^{nom}} \right) \cdot e^{j\phi_{ss}} \quad (2)$$

where:

S_i^{nom}: Apparent nominal power of the *i-th* transformer;

S_{calc}: Apparent power estimated for the feeder root node;

ϕ_{ss}: Angle, in radians, of the power factor measured at the feeder root node;

nt: Total of installed transformer in the feeder;

λ_i: Average loading of the *i-th* transformer obtained from the customer bills or using any other empirical or deterministic method.

The apparent power measured at the feeder root node cannot be directly used in equation (2) because the measured power is composed by the summation of transformers demand and losses. The fault location algorithm

should simulate the same operation conditions as much steady state as during the fault. Depending on the adopted load model the algorithm could not simulate such conditions. The procedure used for estimating the transformer power rating is depicted in figure 2.

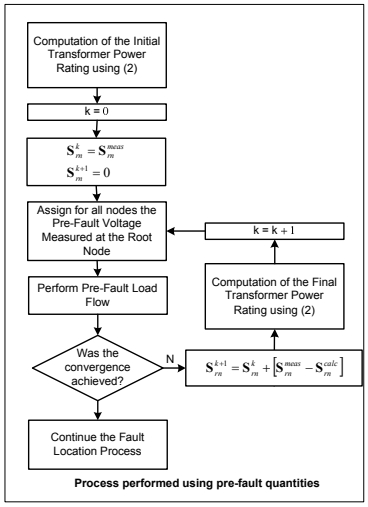

Figure 2: Procedure for estimating the transformer power rating.

The following assumptions should be observed related to figure 2:

- The root node voltage is equal to the measured voltage at this node;
- The initial estimate of the transformer power rating is computed by means of equation (2) considering $S_{calc} = S_{rn}^{meas}$;
- In the first iteration, the voltage for all nodes is equal to the root node voltage;
- The convergence is reached when both inequalities $\left|\mathrm{Re}\left\{\mathbf{I}_{rn}^{meas}\right\} - \mathrm{Re}\left\{\mathbf{I}_{rn}^{calc}\right\}\right| \le \varepsilon$ and $\left|\mathrm{Im}\left\{\mathbf{I}_{rn}^{meas}\right\} - \mathrm{Im}\left\{\mathbf{I}_{rn}^{calc}\right\}\right| \le \varepsilon$ are satisfied;
- S_{rn}^{calc} is calculated using the pre-fault phasors of voltage and current computed by the load flow;
- The final estimate of the transformer power rating is computed by means of equation (2) with $S_{calc} = S_{rn}^{k+1}$;

$\mathbf{S}_{rn}^{meas}$ is computed using the pre-fault phasors of voltage and current measured at the feeder root node.

2.5 During-fault load flow

In the load flow algorithm presented in [3], the root node is the reference node, and the voltage magnitudes and phase angles are known. In order to start the load flow algorithm the voltage for all nodes is equal to the root node. In the fault location algorithm the reference node voltage is equal to the measured voltage at the feeder root node. The iterative process of the load flow algorithm for radial feeders basically consists in the following steps:

i. Compute the injected current at each node;

ii. Perform a backward sweep for calculating the branch currents, i. e., starting from the line section of the last layer and moving towards feeder root node;

iii. Perform a forward sweep for updating the nodal voltages, i. e., starting from the first layer and moving towards the last layer.

Once the above steps have been executed the convergence is checked.

In [3] the equations for calculating the current injections and for checking the convergence have been defined only based on loads of constant power. Since the fault location algorithm must consider a suitable load modeling such equations must be defined again. Based on equation (1), the computation of the during-fault current injections is defined by equation (3) and the convergence checking is defined by equation (4) as follows:

$$\mathbf{I}_{df,jk}^{(n)} = \left(P_{jk} \cdot \left| \frac{\mathbf{V}_{df,jk}^{(n-1)}}{\mathbf{V}_n} \right|^{np} + jQ_{ja} \cdot \left| \frac{\mathbf{V}_{df,jk}^{(n-1)}}{\mathbf{V}_n} \right|^{nq} \right)^{*} - \mathbf{Y}_{jk} \cdot \mathbf{V}_{df,jk}^{(n-1)} \quad (3)$$

$$\mathbf{S}_{df,jk}^{(n)} = \mathbf{V}_{df,jk}^{(n)} \cdot \left(\mathbf{I}_{df,jk}^{(n)}\right)^{*} - \left(P_{jk} \cdot \left| \frac{\mathbf{V}_{df,jk}^{(n-1)}}{\mathbf{V}_n} \right|^{np} + jQ_{ja} \cdot \left| \frac{\mathbf{V}_{df,jk}^{(n-1)}}{\mathbf{V}_n} \right|^{nq} \right) - \mathbf{Y}_{jk} \cdot \left| \mathbf{V}_{df,jk}^{(n-1)} \right|^2 \quad (4)$$

where:

P: active power calculated according to subsection *2.4*;

Q: reactive power calculated according to subsection *2.4*;

$\mathbf{V}_n$: Nominal voltage;

$\mathbf{V}_{df}$: During-fault voltage;

$\mathbf{Y}$: Shunt admittance;

k: phase *a*, *b* or *c*;

j: Feeder node;

n: Load flow iteration index.

2.6 Fault current computation

Figure 3 illustrates a three-phase-to-ground fault occurring at node *m* in a distribution feeder with loads connected at nodes *j* and *k*. Nodal voltages and load currents, computed by means of load flow, as well as the total during-fault current measured at the feeder root node is assumed to be known during the fault location algorithm execution.

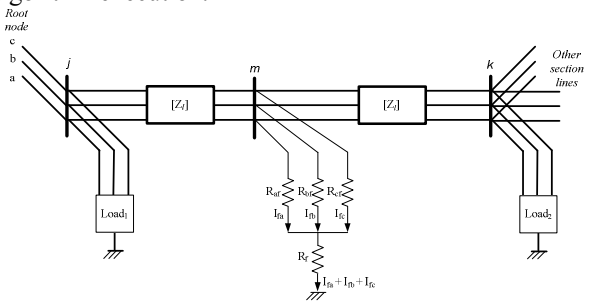

Figure 3: Distribution feeder with a three-phase-to-ground fault at node *m*.

Using the measured currents at the feeder root node, the fault type is defined. For each algorithm iteration, the fault current is computed using the following equation:

$$\mathbf{I}_f = \mathbf{I}_{rn}^{df,meas} - \sum_{i=1}^{nt} \mathbf{I}_i \quad (5)$$

where:

$\mathbf{I}_{rn}^{df,meas}$: During-fault current measured at the feeder root node;

$\mathbf{I}_i$: Load current of transformer *i*;

nt: Total of transformer installed in the feeder.

An important characteristic of the proposed fault location algorithm is that a fault is handled as a load connected in the feeder. In each iteration, the fault current, calculated by means of equation (5) is injected, as proposed in [3], in the analyzed node. The usage of current injection eliminates any assumption related to the fault impedance because it does not configure in the fault modeling.

2.7 Selection of the likely fault location

The likely fault location is selected taking into account all analyzed nodes during the fault location process. For each analyzed node, the during-fault magnitude deviation between measured and calculated voltage sags is computed. Considering the phases involved in the fault, the during-fault sag magnitude deviations are given by:

$$\begin{aligned} &\delta_k^{i,j} = V_{k,meas}^{i} - V_{k,cal}^{i,j} \\ &i = 1,...,mp \\ &j = 1,...,an \end{aligned} \quad (6)$$

where:

$V_{k,meas}^{i}$: Voltage sag magnitude, for phase *k*, measured at node *i* for a fault occurring in the feeder;

$V_{k,calc}^{i,j}$: Voltage sag magnitude calculated for node *i*, for phase *k,* considering a fault simulated at node *j*;

mp: Number of measurement points along the feeder;

an: Total of analyzed nodes.

Equation (6) gives three voltage sag magnitude deviations for a fault involving three phases; two voltage sag magnitude deviations for a fault involving two phases; and one voltage sag magnitude deviation for a single line-to-ground fault. Taking into account that the quantity of magnitude deviations is proportional to the fault type, number of analyzed nodes and number of measurement points there is the necessity of converting the magnitude deviations into a single index for selecting the fault location node. Thus, in order to select the likely fault location, the following steps are executed:

i) Using equation (6), compute all $\delta_k^{i,j}$;

ii) For the same phase *k* and analyzed node *j*, select the bigger and the smaller $\delta_k^{i,j}$ among the measurement points *i*;

iii) For each phase *k* and analyzed node *j*, compute the difference between the bigger and the smaller $\delta_k^{i,j}$;

iv) Considering the differences for phases *a*, *b* and *c*, the fault location index γ, for the analyzed node *j*, is defined as being the bigger difference.

The likely fault location is the node presenting the smaller γ, and the fault area is defined by means of a crescent ordering of the γ_j. The likely faulted node is defined as being that one presenting the smallest γ.

2.8 Convergence criterion

The analysis of each node is made in an iterative way and the convergence is reached when both inequalities in equation (7) are satisfied.

$$\begin{aligned} &\left|\mathrm{Re}\left\{\mathbf{I}_{rn}^{df,meas}\right\} - \mathrm{Re}\left\{\mathbf{I}_{rn}^{df,calc}\right\}\right| \le \varepsilon \\ &\left|\mathrm{Im}\left\{\mathbf{I}_{rn}^{df,meas}\right\} - \mathrm{Im}\left\{\mathbf{I}_{rn}^{df,calc}\right\}\right| \le \varepsilon \end{aligned} \quad (7)$$

where:

$\mathbf{I}_{rn}^{df,meas}$: Current measured at the feeder root node;

$\mathbf{I}_{rn}^{df,calc}$: Current calculated for the feeder root node;

ε: Specified tolerance.

3 SIMULATION RESULTS

An overhead, three-phase, three wire, 13.8 kV, 238-node, practical feeder, illustrated in figure 4 is used for evaluating the proposed fault location algorithm. Figure 4 is non-scale and the furthest node is located at 5600.8 meters from the substation.

3.1 Modelling of lines and loads

Distribution lines are considered as being non-transposed. In-series *RL* model was used and shunt capacitances are neglected in the ATP [4] simulations as well as in the fault location algorithm. Loads are modeled as constant impedances in the ATP simulations. Load model described in subsection *2.3* is employed by the fault location algorithm.

3.2 Fault simulations

Aiming to analyze the accuracy and robustness of the proposed algorithm, faults are simulated in several nodes of the feeder taking into account different transformer loadings, different fault resistances as well as different types of faults. Since the single line-to-ground faults occur more frequently, the presented results are regarding to this fault type. Data generated by ATP simulations are considered as input data to the algorithm. Table 1 contains the parameters for some ATP simulations taking into account transformers with nominal loading.

Table 1: ATP simulation parameters

Node	Fault type	Fault Resistance (Ω)
66, 97, 148, 166, 176, 180	AN	1.0, 5.0, 10.0, 15.0, 20.0

3.3 Points of Voltage Sag Measurements along the feeder

The fault location is carried out using five voltage sag meters placed along the feeder at nodes 11, 109, 166, 176 and 225.

3.4 Impact of the transformer power rating in the accuracy of the fault location algorithm.

As presented in subsection *2.4*, the fault location algorithm estimates the transformer power rating using the complex power measured at the feeder root node and the nominal power of the transformers installed in the feeder. Therefore, each transformer will have the same

loading percentage in relation to its nominal power. However, each customer has different power demand reflecting in a stochastic behavior of the transformer loading. Then, the several transformers installed in the feeder have different loadings at the moment of the fault occurrence.

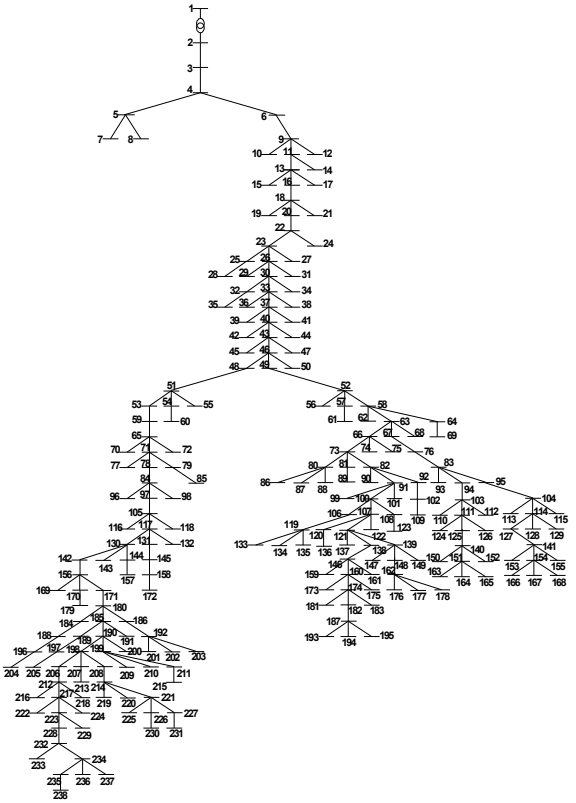

Figure 4: Practical feeder used for assessing the fault location algorithm.

ATP simulations considering a random power rating for each transformer are carried out in order to aim to assess the impact of the uncertainness of the transformer power ratings. Thus, the complex power of each transformer used in the ATP simulation is given by:

$$\mathbf{S}_i^{ATP} = \xi_i \cdot S_i^{nom} \cdot e^{j\phi} \qquad (9)$$

where:

ξ_i: Random variable;

S_i^{nom}: Nominal apparent power of the *i-th* transformer;

ϕ: Angle, in radians, of the power factor adopted for the transformer.

According to (9), for the *i-th* transformer, the deviation between the nominal apparent power and the loading used in the ATP simulation reduces when the standard deviation goes towards zero. Figures 5 and 6 show the random variable ξ chosen from a normal distribution of mean one with σ = 0.3 and σ = 0.7.

Single line-to-ground faults are simulated at several nodes of the feeder considering the fault resistances listed in table 1. The transformer power rating used in the fault location algorithm is estimated according to subsection *2.4* and constant impedance load model is used. The following results are related to the choice of σ = 0.7, since it produces a bigger deviation between the nominal apparent power and the loading transformer used in ATP simulations than choosing σ = 0.3. For node 176 the fault location algorithm pinpointed this same node as the faulted node. For node 180 the fault location algorithm pinpointed this same node as the faulted node excepting the simulations using fault resistances of 15.0 and 20.0 Ω and σ = 0.7. Figures 7 and 8 show the fault location index γ, ranked in a crescent ordering and the distance between the actual faulted node and the analyzed node by the algorithm.

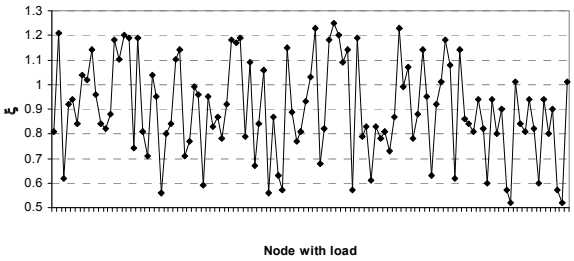

Figure 5: Random variable ξ with σ = 0.3.

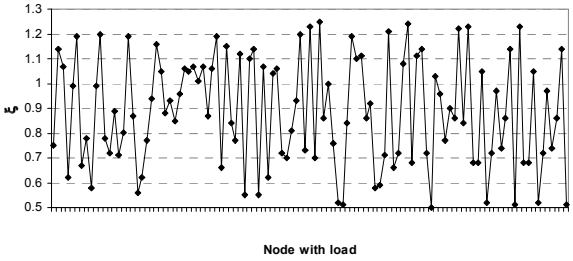

Figure 6: Random variable ξ with σ = 0.7.

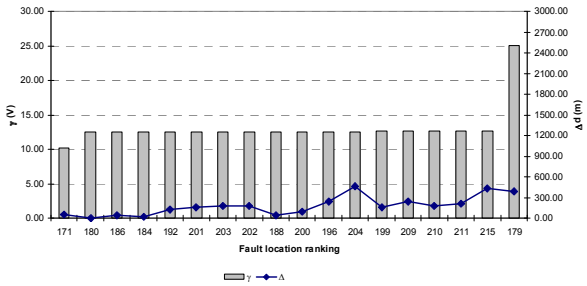

Figure 7: Fault location ranking and distance between the actual faulted node and the analyzed node for a fault at node 180 with fault resistance 15.0 Ω.

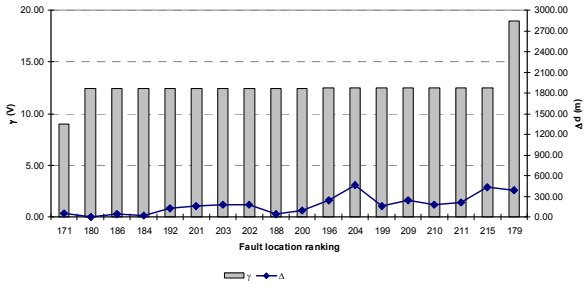

Figure 8: Fault location ranking and distance between the actual faulted node and the analyzed node for a fault at node 180 with fault resistance 20.0 Ω.

In the above figures, the actual faulted node is ranked at the second position. The distance between this node and the node ranked at the first position is 55.0 meters. It could be noted that the nodes ranked from the second position to the sixteenth position can delimit a faulted zone containing the faulted node. In this zone, the furthest node of the actual faulted node is located at 460.7 meters. The node 180 is located at 4082.6 meters from the substation and the node 204 is located at 4543.3 meters from the substation.

3.5 Impact of the load model in the accuracy of the fault location algorithm.

Aiming to assess the impact of the uncertainties in the load model in the robustness and accuracy of the fault location algorithm, six different pairs of the load exponents *np* and *nq*, equations (3) and (4), are used. The used pairs of load exponents are listed in table 2.

Table 2: Pairs of exponents used for assess the impact of the uncertainties of the load model in the algorithm accuracy

np	1.0	1.2	1.3	1.5	1.7	1.8
nq	1.8	3.0	4.5	4.0	5.5	6.0

All nodes presented in figure 4 are analyzed by the algorithm during the fault location process for faults at nodes listed in table 1. In the fault location process, the power rating of each transformer is calculated as described in subsection *2.4* taking into account the average loading equal to the nominal power, i.e., $\lambda = 1.0$. The algorithm have pinpointed with accuracy the majority of the fault locations and minors errors are observed for locating faults at nodes 66, 97, 148 and 166. Following these errors are presented and discussed.

Figure 9 shows the fault location index γ, ranked in a crescent ordering and the distance between the faulted node 66 and the analyzed node by the algorithm using *np* = 1.3 and *nq* = 4.5. This fault is simulated in ATP using fault resistance equal 20.0Ω.

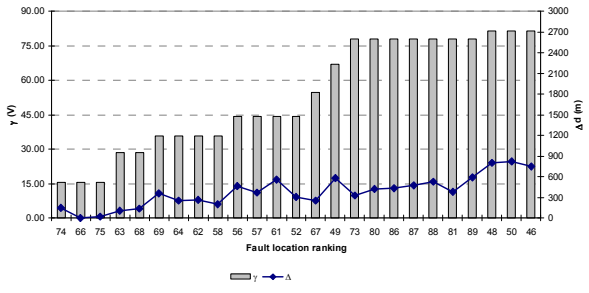

Figure 9: Fault location results for a fault simulated at node 66 with fault resistance equal 20.0 Ω in the ATP, and *np* = 1.3 and *nq* = 4.5 in the fault location algorithm.

It can be noted from figure 9 that node 66 is ranked at second position. The node 74 is located at 148.2 meters far from node 66. This error is quite acceptable since the node 74 is the receiving node of the line section that has the node 66 as sending node. Additionally, the fault location indices of the three first nodes present almost the same value delimiting a faulted area containing the actual faulted node.

Figure 10 shows the fault location index ranked in a crescent ordering and the distance between the faulted node 97 and the analyzed node by the algorithm using *np* = 1.2 and *nq* = 3.0. This fault is simulated in ATP using fault resistance equal 1.0Ω.

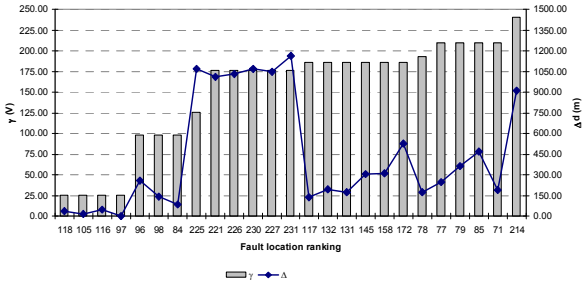

Figure 10: Fault location results for a fault simulated at node 97 with fault resistance equal 1.0 Ω in the ATP, and *np* = 1.2 and *nq* = 3.0 in the fault location algorithm.

It can be noted from figure 10 that node 97 is ranked at forth position. The node 118 is located at 37.4 meters far from node 97. This error is perfectly acceptable since the fault location indices of the forth first nodes present the same value delimiting a faulted area containing the actual faulted node.

Figure 11 shows the fault location indices ranked in a crescent ordering and the distance between the faulted node 148 and the analyzed node by the algorithm using *np* = 1.8 and *nq* = 6.0. This fault is simulated in ATP using fault resistance equal 20.0Ω.

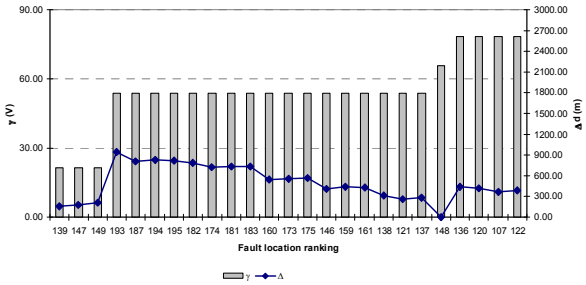

Figure 11: Fault location results for a fault simulated at node 148 with fault resistance equal 20.0 Ω in the ATP, and *np* = 1.8 and *nq* = 6.0 in the fault location algorithm.

It can be noted from figure 11 that node 148 is ranked at twenty-first position. The node 139 is located at 158.4 meters far from node 148. Even the actual faulted node being ranked at twenty-one position, this error is acceptable because the node 139 is the sending node of the line section that has the node 148 as receiving node. Additionally, the fault location indices of the three first nodes of the ranking present the same value delimiting a likely faulted area. This area does not contain the actual faulted node, but nodes 147 and 149 are connected to the node 148 through two line sections.

Figure 12 shows the fault location indices ranked in a crescent ordering and the distance between the faulted node 166 and the analyzed node by the algorithm using *np* = 1.7 and *nq* = 5.5. This fault is simulated in ATP using fault resistance equal 10.0Ω.

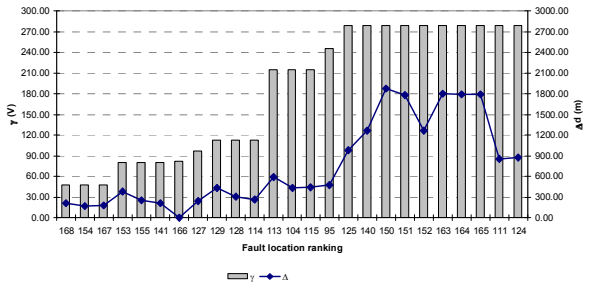

Figure 12: Fault location results for a fault simulated at node 166 with fault resistance equal 10.0 Ω in the ATP, and *np* = 1.7 and *nq* = 5.5 in the fault location algorithm.

It can be noted from figure 12 that node 166 is ranked at seventh position. The node 168 is located at 207.8 meters far from node 166. Again, this error is acceptable because the sixth first nodes of the ranking are in the same geographical area of the feeder ensuring the indication of the right direction that the maintenance crews must go in order to find the faulted point and execute the necessary repairs.

4 CONCLUSIONS

A robust and efficient algorithm using sparse measurements of voltage sag magnitudes for fault location in distribution feeders is presented and discussed. The algorithm can be implemented with few additional investments by most of electric utilities. The main requirements of the algorithm are devices for measurements of voltage and current at the feeder root node and voltage measurements at some feeder nodes along with communication channels for transmitting the recorded quantities to the computer responsible for processing the fault location algorithm.

The test results show that the algorithm is a useful tool for aiding in the fault location process, mainly when the faulted points are difficult to be found only by visual inspection such as insulator failures or trees touching the network. Thus, the proposed algorithm is an excellent auxiliary tool for indicating to the maintenance crews the right direction of the fault in the feeder. Then, the time for search of the faulted point, the reparation time as well as the supply restoration time can be minimized enhancing the reliability and quality indices related to these times.

ACKNOWLEDGEMENTS

The first author gratefully acknowledges the Visiting Researcher Position, as well as the facilities support provided by the Electric and Computer Engineering Department at Texas A&M University from November, 2005 to August, 2006. The authors would like to acknowledge the financial support received from Capes – Brazil (grant nº BEX0769/05-3), FEPISA (grant nº 007/2005) and CNPq – Brazil (grant nº 301060/2006-1).

REFERENCES

[1] Abur, A. and Z. Galijasevic, "Fault location using voltage measurements". *IEEE Transactions on Power Delivery*, vol. 17, nº 2, p.441 – 445, 2002.

[2] Aggarwal, R. K., Y. Aslan and A. T. Johns, "New concept in fault location for overhead distribution systems using superimposed components", *IEE Proceedings Generation, Transmission and Distribution*, vol. 144, nº 3, pp. 309 – 316, 1997.

[3] Cheng, C. S. and D. Shirmohammadi, "A three-phase power flow method for real-time distribution system analysis", *IEEE Transactions on Power Systems*, vol. 10, nº 2, pp. 671 – 679, 1995.

[4] Comite Argentino de Usuarios del EMTP/ATP, "ATP Rulebook", Argentina, 2002.

[5] El-Hami, M., L. L. Lai, D. J. Daruvala, and A. T. Johns, "A new traveling-wave based scheme for fault detection on overhead power distribution feeders", *IEEE Transactions on Power Delivery*, vol. 7, nº 4, pp. 1825 – 1833, 1992.

[6] Girgis, A. A. and C. M. Fallon, "Fault location techniques for radial and loop transmission systems using digital fault recorded data", *IEEE Transactions on Power Delivery*, vol. 7, nº 4, pp. 1936 – 1945, 1992.

[7] Gohokar, V. N. and M. K. Khedkar, "Faults locations in automated distribution system", *Electric Power Systems Research*, vol. 75, pp. 51 – 55, 2005.

[8] Jarventausta, P., P. Verho and J. Partenen, "Using fuzzy sets to model the uncertainty in the fault location process of distribution networks", *IEEE Transactions on Power Delivery*, vol. 9, nº 2, pp. 954 – 960, 1994.

[9] P. Kundur, "Power System Stability and Control", USA, McGraw-Hill, 1994.

[10]Li, H., A. S. Mokhar and N. Jenkins, "Automated fault location on distribution network using voltage sags measurements", *Proc. of the 18th International conference and Exhibition on Electricity Distribution, CIRED*, 2005.

[11]Luo, S., M. Kezunovic and D. R. Sevick, "Locating faults in the transmission network using sparse field measurements, simulation data and genetic algorithm", *Electric Power Systems Research*, vol. 71, nº 2, pp. 169 – 177, 2004.

[12]Pereira, R. A. F. et al., "Location of single line-to-ground faults on distribution feeders using voltage measurements" *IEEE/PES Proceedings of the Latin América Transmission and Distribution Conference and Exposition*, 2006.

[13]Senger, E. C et al., "Automated fault location system for primary distribution networks", *IEEE Transactions on Power Delivery*, vol. 20, nº 2, pp. 1332 – 1340, 2005.